Airfoil Performance in Heavy Rain

JAMES R. VALENTINE

In recent years microbursts have been implicated in several major aviation accidents. Since microbursts are often accompanied by heavy rainfall, an interest in airfoil performance in rain has arisen. As raindrops strike the leading edge of an airfoil, small droplets are splashed back into the airflow field, and an uneven water film forms on the airfoil surface. Both phenomena have been hypothesized to contribute to a degradation of airfoil performance in rain that may be manifested as a decrease in lift, an increase in drag, and premature stall. The splashed-back droplets are accelerated by the airflow field. Thus droplet drag acts as a momentum sink to deenergize the boundary layer, while the uneven water film effectively roughens the airfoil surface. A numerical, two-way momentum coupled, two-phase flow scheme for the evaluation of the effect of splashed-back droplets on a NACA 64-210 airfoil section in cruise configuration is described. A thin-layer Navier-Stokes computational fluid dynamics code is coupled with a Lagrangian particle tracking scheme to determine the two-phase flow field in an iterative manner. Noninteracting, nondeforming, and nonevaporating spherical particles representing statistical distributions of raindrops are tracked through the curvilinear body-fitted grid used by the airflow code. A simple model is used to simulate raindrop impacts and the resulting splashback on the airfoil surface. Results are compared with wind tunnel test results.

On July 9, 1982, Pan American World Airways Flight 757, a Boeing 727, encountered a microburst upon taking off from New Orleans International Airport and crashed, killing 153 persons. Estimates of rainfall rates encountered by the aircraft range up to 144 mm/hr (*1*). Serious investigations of heavy rain effects on aircraft performance had begun only a few years earlier, and researchers reported that significant airfoil performance penalties (decreased lift, increased drag, and earlier stall) may occur at rainfall rates of 150 mm/hr or greater (*1*). The primary cause of the accident was the microburst wind patterns, but it was unknown whether rain had also played some role. It is possible that a rain-induced premature aerodynamic stall could occur before the aircraft stall warning system was activated. Concern over this accident led to a Federal Aviation Administration (FAA) and National Academy of Sciences (NAS) study of the hazards of wind shear for aircraft that are landing or taking off (*2*). The study analyzed 27 wind shear–related aircraft accidents and incidents that had occurred between 1964 and 1982 and concluded that the most dangerous types of wind shears are the downdraft and outflow microbursts associated with convective storms. Since these storms are often accompanied by heavy rainfall, one of the report's recommendations was the continued investigation of the aerodynamic performance of aircraft in heavy rain. The most recent analysis of aircraft performance in heavy rain (*3*) had been developed from experimental studies of rough airfoils and low-speed water drop splashes and had not been validated by wind tunnel simulations of airfoils or aircraft in rain.

Department of Mechanical Engineering, University of Utah, Salt Lake City, Utah 84112.

AIRFOIL AERODYNAMICS

A typical streamline pattern around an airfoil at a relatively low angle of attack (α) is shown in Figure 1a. As α is increased, lift also increases until a maximum is reached at the stall angle of attack (α_{stall}). At stall, there is a rapid decrease in lift and an increase in drag due to massive separation of the flow on the upper surface of the airfoil, as shown in Figure 1b. The airfoil shown in Figure 1 is in cruise configuration; for landing and taking off, leading edge slats and trailing edge flaps are extended to increase lift and to delay stall to a higher angle of attack. In this paper, lift and drag are measured in terms of the normalized (or nondimensionalized) quantities, lift and drag coefficiencts (c_l and c_d).

Experimental results have indicated that an airfoil in heavy rain may be subject to a decrease in maximum lift, an increase in drag, and earlier onset of stall (at a lower α). These effects are most pronounced in high lift configurations with flaps and slats deployed. Since high lift configurations are used in takeoffs and landings when there is little margin for error, the adverse effects of rain may have the most serious consequences in these cases. It is unlikely that heavy rain by itself will cause an accident. However, it may be a contributing cause when other factors such as wind shears are present.

MICROBURSTS

A microburst is a short-lived, thunderstorm-induced local downdraft. As the vertical downdraft winds encounter the ground, a strong horizontal outflow is produced around the downdraft core. Initially, an aircraft encountering a microburst experiences a strong headwind and increases in airspeed and lift as it enters the outflow region, possibly prompting the pilot to decrease thrust or pitch or both. After the aircraft passes the downdraft area, however, the outflow becomes a tail wind, and the resultant decrease in airspeed causes a decrease in lift, often with dire consequences if the aircraft is landing or taking off and especially if thrust or pitch was reduced on the initial headwind encounter. In a study of 75 microbursts the average change in wind velocity encountered by the aircraft was 47 knots, whereas a maximum of almost 100 knots was measured (*4*). It was estimated that the aircraft experienced this velocity change over 20 to 40 sec. Microbursts are often accompanied by heavy rainfall. Thus flight through a microburst may be complicated by the adverse effects of rain on aircraft aerodynamics.

HEAVY RAIN ACCIDENTS

Other accidents and incidents in addition to the Pan American World Airways Flight 757 accident have occurred during very heavy rainfall. Several before 1982 are mentioned by Luers and

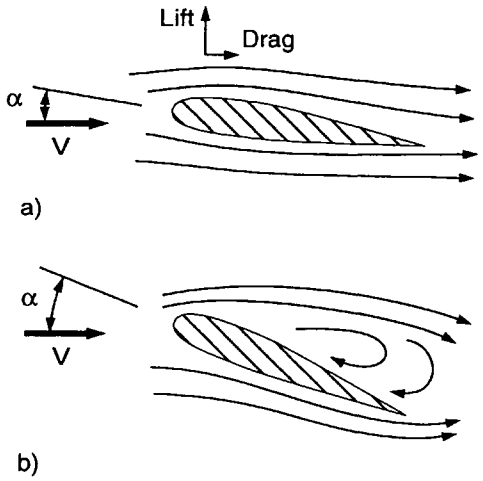

FIGURE 1 Streamline patterns for the flow around an airfoil in cruise configuration: (*a*) airfoil at low angle of attack (α), (*b*) stalled airfoil at high angle of attack (α).

Haines (*5*) and two of these, an Eastern Airlines Flight 066 accident at JFK International Airport on June 24, 1975, and an Eastern Airlines Flight 693 incident at William B. Hartsfield Atlanta International Airport on August 22, 1979, are analyzed. In both cases, Luers and Haines estimate that the aircraft involved may have encountered rainfall rates of 300 mm/hr. These rates could induce a significant aerodynamic performance penalty. However, in neither case did the National Transportation Safety Board (NTSB) report account for rain effects. Another accident occurred on August 2, 1985, when Delta Airlines Flight 191 crashed after encountering a microburst during an intense thunderstorm as it approached Dallas–Fort Worth International Airport for landing. Weather radar indicated a rainfall rate of up to 114 mm/hr, and witnesses described the aircraft as emerging from a wall or curtain of water immediately before ground impact (*4*). Brandes and Wilson (*6*) report that it is not uncommon for radar measurements of rainfall rates to be in error by more than a factor of two and found that in heavy rainfall radar may underestimate the rainfall rate. Thus, a rainfall rate of 114 mm/hr may be less than that actually encountered by the aircraft.

Luers and Haines (*5*) suggest that pilots be made aware of the possibility that aerodynamic stall can occur in heavy rain above the usual stall speed and before the aircraft stall warning system activates. They advise that high angle of attack microburst recoveries, which sacrifice airspeed for altitude, be avoided in favor of an attempt to increase airspeed at a slower climb rate, thus avoiding a rain-induced premature stall. Although they are somewhat controversial, such high angle of attack recoveries have been recommended to pilots of jet-powered aircraft in microburst encounters (*7*).

PHYSICS OF AN AIRFOIL IN RAIN

Several mechanisms have been hypothesized as contributing to the degradation of airfoil (or aircraft) performance in heavy rain. The main ones are the loss of aircraft momentum due to collisions with raindrops, the effective roughening of the airfoil surface due to the presence of an uneven water layer, and the loss of boundary layer air momentum due to the splashback of droplets into the airflow field as raindrops strike the airfoil surface. Bilanin (*8*) has also considered the evaporation of droplets near the airfoil surface and concluded that this process does not significantly affect airfoil performance.

This paper describes a numerical scheme to model the loss of boundary layer air momentum due to splashed-back droplets. As raindrops strike an airfoil, and "ejecta fog" of splashed-back droplets forms at the leading edge, as shown in Figure 2. It has been hypothesized that the acceleration of these droplets in the boundary layer by the airflow field may act as a momentum sink for the boundary layer, resulting in a decreased airflow velocity. Deceleration of the boundary layer can lead to a loss of lift, premature separation and stall, and an increase in drag. By evaluating the boundary layer momentum sink (or source) term, modifications of the boundary layer flow and the resulting change in airfoil performance can be evaluated.

Beneath the ejecta fog layer, a thin water film forms on the airfoil surface because of the fraction of the raindrop that is not splashed back. The thickness of the water film has been measured in small-scale wind tunnel investigations to be of the order of 0.1 mm or less (*10*) and has been estimated at full scale to be about 1 mm or less (*11*). Raindrop impact craters and suface waves in the water film effectively roughen the airfoil surface. The adverse effect of this rougher surface on aerodynamic performance has been analyzed in detail by Haines and Luers (*11*). As the water film is carried downstream, rivulets form on the back portion of the airfoil. With increasing angle of attack, the extent of the water film decreases on the upper surface and increases on the lower surface. When stall is reached, the rivulets disappear and pooling of water occurs on the separated portion of the airfoil.

CHARACTERISTICS OF RAIN

Ground-level rainfall rates are generally measured in terms of millimeters or inches of water accumulation per hour. The heaviest recorded ground rainfall occurred during an intense thunderstorm in Unionville, Maryland, on July 4, 1956, when a rainfall rate of 1874 mm/hr was recorded for a period of approximately 1 min

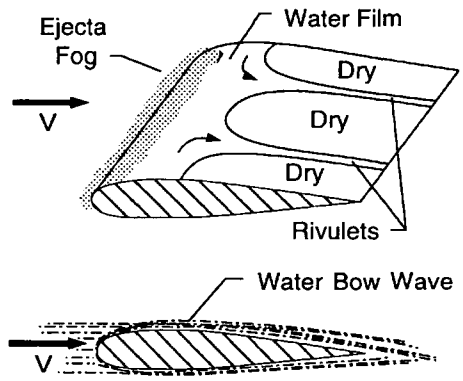

FIGURE 2 A cruise-configured airfoil in rain showing the ejecta fog and water surface film (*9*).

(*12*). Typically, ground-level rainfall rates are much lower than this, with the heaviest rainfalls occurring for short periods of 30 sec or less. Dunham (*13*) has estimated that at any location in the subtropical maritime southeastern United States, a total of approximately 2 min of 200 mm/hr or heavier rainfall can be expected during 1 year.

During a thunderstorm, significantly higher rain intensities than those at ground level can be expected at a higher altitude. The rain measurement parameter used above ground level is liquid water content (LWC) or the mass of water per unit volume of air. LWC is also important in wind tunnel testing, since the same value must be used in small-scale tests as is measured in an actual rainstorm (*8*). Roys and Kessler (*14*) have taken airborne measurements of LWC within several Great Plains thunderstorms and reported an average value of 8.7 g/m^3 and a peak value of 44 g/m^3. At the time and location of the peak airborne measurement, however, ground-based radar indicated a rainfall rate of only 37.6 mm/hr (corresponding to an LWC of about 1.14 g/m^3), possibly because of the small size of the region of extremely intense rain.

The drop size distribution of ground-level rain can be approximated by the expression

$$N(D_p) = N_0 \exp(-\Lambda D_p) \quad (1)$$

where $N(D_p)$ is the number of raindrops of diameter D_p (in mm) per cubic meter of air per diameter interval and N_0 and Λ are empirically determined parameters dependent on rainfall rate and the type of rainstorm. (*15*). Marshall and Palmer's (*15*) values of $N_0 = 8 \times 10^3$ m^{-3}mm^{-1} and $\Lambda = 4.1 \times R^{-0.21}$, where R is the rainfall rate (mm/hr), have been used commonly for continuous rain, but values of $N_0 = 1.4 \times 10^3$ m^{-3}mm^{-1} and $\Lambda = 3.0 \times R^{-0.21}$ have been found more appropriate for heavy thunderstorm rain (*16*). Raindrop diameters generally range up to about 6 or 7 mm with the larger drop sizes most prevalent in heavier rainfalls.

A relationship between LWC and ground-level rainfall rate can be derived by multiplying the raindrop diameter distribution given by Equation 1 by the mass of the raindrop, then integrating over the range of drop diameters. Assuming a maximum raindrop diameter of 7 mm, the average LWC of 8.7 g/m^3 measured by Roys and Kessler (*14*) corresponds to a rainfall rate of about 546 mm/hr at ground level. In experimental and analytical analyses of aircraft performance in heavy rain, LWCs corresponding to rainfall rates of 500 mm/hr to 2000 mm/hr are commonly used.

HISTORY OF AIRCRAFT HEAVY RAIN STUDIES

The first study of heavy rain effects on aircraft flight was performed by Rhode (*17*) in 1941. He concluded that the most severe performance penalty experienced by a DC-3 flying through a rainstorm with LWC of 50 g/m^3 was due to the loss of aircraft momentum caused by collisions with raindrops. It was estimated that this effect could result in a decrease in airspeed of up to 18 percent, but the duration of the rain would not be sufficient to pose a significant hazard to an aircraft at a cruising altitude of 5,000 ft. Aircraft landing and taking off in heavy rain were not considered; these operations were not routine at that time during low-visibility conditions. Rhode recognized that the surface of the aircraft may be effectively roughened by rain but noted that insufficient test data existed to evaluate this effect.

The current interest in heavy rain effects began with reports by Luers and Haines (*3,5,11*) in 1982. Four mechanisms that could potentially degrade aircraft or airfoil performance in heavy rain were identified: (*a*) the momentum lost by the aircraft due to collisions with raindrops, (*b*) the added weight of a thin water film on the surface of the aircraft, (*c*) the added roughness due to the uneven surface of the water film, and (*d*) a change in pitching moment caused by raindrops striking the aircraft unevenly. The first three were analyzed, and the third appeared to have the most effect on aircraft performance. The added weight of a water film was inconsequential, and the loss of aircraft momentum due to raindrop impacts may be measurable for an aircraft landing or taking off in a torrential rainfall but would not present a significant hazard by itself. However, an effectively rougher aircraft surface due to an uneven water film could have a profound effect on the performance of the aircraft. Estimates of this effect on the aerodynamic performance of a Boeing 747 for various rainfall rates were made. By assessing the roughness of the water layer and comparing the results with correlations for flat plates and airfoils with fixed roughness elements (which were not available at the time of Rhode's study), the increase in drag, decrease in maximum lift, and decrease in stall angle of attack were evaluated. Appraisals of aircraft performance penalties were made for rainfall rates varying from 100 to 2000 mm/hr. Estimates of drag increases ranged from 5 to 30 percent, decreases in maximum lift from 7 to more than 30 percent, and decreases in stall angle of attack from 1 to 6 degrees. The highest penalties were predicted for the highest rainfall rates.

During the last 10 years, wind tunnel investigations of heavy rain effects on airfoil performance in rain have been conducted. There have been two main categories of investigations: those in which the boundary layer on the dry airfoil is predominantly laminar and those in which the boundary on the dry airfoil is tripped to turbulence near the leading edge. The rain effect on a laminar flow airfoil has been mimicked by tripping the boundary layer to turbulence on the dry airfoil, whereas the rain effect on an airfoil with a turbulent boundary layer appears to result from premature flow separation.

An early laminar boundary layer test was conducted with a Rutan VariEze, a small canard-configured sport aircraft (*18*). Pilots of similar aircraft had reported control difficulties in rain (*19*). The canard surface is used for pitch control and is designed to promote laminar flow. It can be very sensitive to any surface roughness that may cause turbulence. In a full-scale wind tunnel investigation, it was discovered that the rain effect is appoximately equivalent to tripping the canard surface boundary layer to turbulence without rain.

Hansman and Barsotti (*20*) examined the performance of a small-scale laminar flow Wortmann FX67-K170 airfoil (similar to those used on sailplanes) with various surface coatings of different wettability in simulated rain. A wettable surface is one on which water spreads out and forms a thin film, whereas an unwettable surface is one on which water tends to form beads. An unwettable surface should develop a larger effective roughness in rain because of the beading effect, and an airfoil with this surface could be expected to sufffer a larger performance penalty. In these experiments, the performance of a waxed (low wettability) Wortmann FX67-K170 airfoil suffered a larger decrease in lift and increase in drag in simulated rain than one with a more wettable unwaxed surface. The rain effect could be partially simulated by tripping the boundary layer to turbulence on the dry airfoil. However, there was also a rain-induced effective change in the camber of the airfoil (evidenced by a decrease in the zero lift angle of attack)

that could not be duplicated with a turbulent boundary layer. This apparent change in airfoil shape may have been a result of the very small scale of the airfoil (6-in. chord length) and the inability to scale the surface film and splashback appropriately.

Hansman and Craig (*21*) conducted small-scale tests of three airfoils at wind tunnel speeds low enough (low Reynolds numbers) that the boundary layer can be assumed predominantly laminar. The three airfoils tested were a NACA 0012 airfoil similar to those used as horizontal stabilizers on general aviation aircraft, a NACA 64-210 airfoil characteristic of the type used for many modern transport aircraft, and a Wortmann FX67-K170 airfoil. At low angles of attack, the performance of each airfoil was degraded in simulated rain, with the Wortmann FX67-K170 airfoil, which is designed for laminar flow, suffering the largest penalty, a decrease in lift of up to 25 percent. This performance loss could be mimicked by tripping the boundary on the dry airfoil to turbulence. The NACA 0012 and NACA 64-210 airfoils both exhibited a delayed stall in rain, a result that could be expected if the laminary boundary layer was tripped to turbulence.

There have also been wind tunnel tests of airfoils with turbulent boundary layers, a condition more closely resembling the actual flow around a general aviation or transport type airfoil. NACA 0012, NACA 64-210, and NACA 23015 airfoil sections and wings have been used in experiments (*9,13,22,23*). The overall results of these tests indicate that an airfoil with a turbulent boundary layer in heavy rain may be subject to a decrease in maximum lift, an increase in drag, and premature stall. The effects are most pronounced in high-lift configurations with flaps and slats deployed.

Typical results are those of Bezos et al. (*9*) for a NACA 64-210 airfoil section in simulated wind tunnel rain. A 2.5-ft-chordlength airfoil section mounted between two endplates was tested in both cruise and high-lift configurations, with the boundary layer tripped to turbulence near the leading edge. In cruise configuration, simulated rain resulted in a decrease in maximum lift of up to 17 percent and an increase in drag at constant lift of up to 71 percent. In high-lift configurations with a leading edge slat and a double-slotted trailing edge flap deployed, a decrease in maximum lift of up to 18 percent, an increase in drag at constant lift of up to 40 percent, and a decrease in stall angle of attack of up to 8 degrees were measured. The airfoil showed a greater sensitivity to rain in the high-lift configuration than in cruise configuration. In general, the largest performance penalties were measured at the highest wind tunnel velocities (largest Reynolds numbers) and for the largest values of LWC. The effect of surface wettability was investigated in the high-lift configuration, but no significant change in the performance penalty was measured, in contrast to the results of Hansman and Barsotti (*20*) for a laminar flow airfoil.

Thus in turbulent boundary layer investigations the airfoil performance penalty in rain is most severe at high angles of attack and appears to be due to a rain-induced premature boundary layer separation that can result from either (or both) an effectively rougher airfoil surface or boundary layer momentum loss to splashed-back droplets. The penalty is more pronounced in high-lift configurations, in heavier rainfalls, and at higher air velocities.

The primary value of small-scale wind tunnel experiments lies in the extrapolation of the results to full scale, and Bilanin (*8*) has examined scaling laws for this purpose. Geometric scaling problems were among several difficulties noted. In small-scale wind tunnel investigations the thickness of the water surface film and the splashback process probably will not be scaled by the same factor as the airfoil itself. Thus the airfoil shape may be effectively changed, as was observed by Hansman and Barsotti (*20*). The water surface film will probably be too thick at small scale. Thus slots between flaps or flaps and the main body of the airfoil will be blocked more than at full scale, possibly resulting in a wind tunnel overprediction of the actual performance penalty in rain. Bilanin (*8*) has shown that the value of LWC must be conserved between small and full scale, but the drop diameters must be scaled. Scaling of drop diameters in a wind tunnel investigation reduces the downward velocity of the raindrops, and this in turn affects the incidence angles and locations where drops strike the airfoil. Because of these scaling difficulties, NASA has developed a facility for large-scale testing of a NACA 64-210 airfoil (with a chord length of 10 ft) at the Langley Research Center (*24*).

In addition to the analytical and experimental studies of airfoil performance in heavy rain, there have been numerical investigations. Calarese and Hankey (*25*) added a body force term to the Navier-Stokes equations because of droplet drag and calculated the resulting pressure distribution on a NACA 0012 airfoil for the two limiting cases of very fine rain (small drop diameters) and very coarse rain (large drop diameters). The flow was treated as a continuous, homogeneous rain-air mixture with a set of conservation laws for each phase. For coarse rain, no appreciable change in performance was determined, but for very fine rain, an increase in lift was predicted because of the increase in density of the mixture over that of air alone. This analysis neglected the effect of splashes and surface roughness, however. Kisielewski (*26*) added a force due to droplet drag to the Euler equations and used a flux vector splitting scheme to solve for the resultant flow field around a NACA 0012 airfoil section. He was unable to duplicate the performance penalty measured experimentally for similar rain conditions, however, and recommended that investigations of the effects of surface roughness and splashback be carried out. Donaldson and Sullivan (*27*) estimated the momentum sink experienced by the boundary layer due to splashed-back droplet drag and added it to a boundary layer code. They concluded that a rainfall rate of 500 mm/hr may be sufficient to induce premature stall of a commercial transport aircraft. Bilanin et al. (*28*) also evaluated the effect of splashed-back droplet drag on the boundary layer and reached a similar conclusion—that this deenergization of the boundary layer could cause an early separation. However, they noted that the effectively rougher surface of the wet airfoil can also play a role in this process and that relative importance of these two mechanisms is unknown.

NUMERICAL METHOD

The numerical scheme used in this project models the two-phase flow of rain (particulate phase) and air (fluid phase) over an airfoil. Two approaches are commonly used to model fluid-particle flows. These models have been reviewed by Decker and Schafer (*29*) and Durst et al. (*30*), among others. The "two-fluid" or Eulerian model treats both the fluid and dispersed particle phases as continuous and solves the appropriate conservation equations for each flow. Interphase exchanges of mass, momentum, and energy are included as source terms in the appropriate conservation equations. This model is most easily implemented when particles are of a uniform size.

The "tracking" or Lagrangian approach involves solving a set of Eulerian conservation equations for the continuous fluid phase, then solving Lagrangian equations of motion to determine particle trajectories. A one-way momentum coupled model assumes that the particle motion is influenced by the fluid phase through drag but that the fluid flow field is unaffected by the presence of particles. A fully two-way coupled model, as used here, accounts for the two-way exchange of momentum (and mass and energy if applicable) between the particle and fluid phases through inclusion of source terms in the fluid conservation equations.

The present model consists of a thin-layer Navier-Stokes code for the calculation of the airflow field and a particle tracking scheme for determination of raindrop trajectories. The two-phase flow field is evaluated with a particle-source-in cell technique (*31*), as shown in Figure 3. The fluid and particle fields are initially calculated, then the fluid phase is updated, this time accounting for particle effects, and the particle trajectories are recalculated in the new fluid flow field. The process is repeated until a stationary solution is reached. Interphase momentum coupling is through drag forces. Drag forces acting on particles influence the particle trajectories, and when sufficient numbers of particles move with velocities other than the fluid velocity, the fluid flow field is influenced by particle drag. Raindrop impacts on the airfoil surface and the resulting breakup and splashback of droplets into the airflow field are modeled in the particle-tracking algorithm.

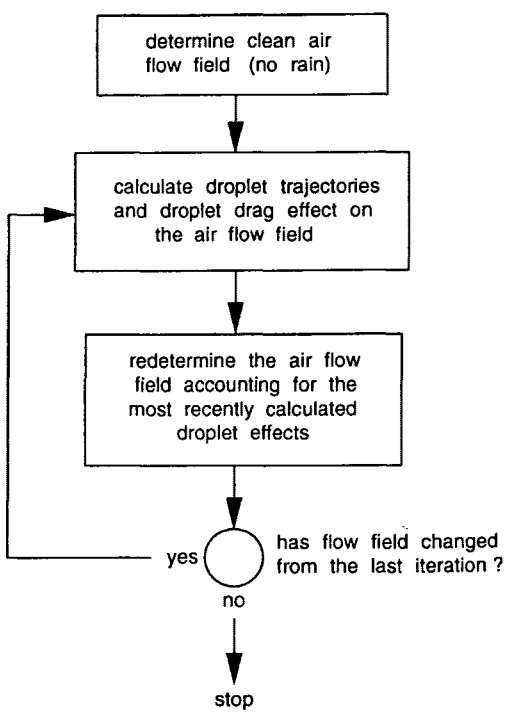

FIGURE 3 Particle-source-in cell algorithm (*31*) for the determination of two-phase particle/fluid flows. Beginning with a clean airflow field (no particles), the particle trajectories and momentum source/sink terms for the airflow field are determined, then the airflow field is updated, accounting for the particle effects. The process is repeated until the fields are unchanged between successive iterations.

Airflow Field Determination

The motion of the fluid (air) phase is governed by the incompressible Navier-Stokes equations. The airflow field is determined with FMC1, a three-dimensional flux-splitting code for the thin-layer approximation of these equations, the details of which have been reported previously (*32*). The code has been modified to account for interphase momentum coupling by adding a momentum source term due to particle drag to the right-hand side of the Navier-Stokes equations.

For numerical determination of the flow field around an arbitrary shape such as an airfoil, a grid that conforms to the body surface is generally used. In this case, an O-H grid is used around a NACA 64-210 airfoil section, a spanwise cross section of which is shown in Figure 4. Grid dimensions are 45 normal to the surface (ξ) by 3 spanwise (η) by 143 circumferential (ζ). This grid defines a curvilinear $\xi\eta\zeta$ coordinate system that is used to track particles. There is no variation of the flow field in the spanwise direction.

Particle-Tracking Algorithm

Raindrops are represented by nonevaporating (no mass coupling between the phases), noninteracting (no collisions between drops), and nondeforming spherical particles (drag on a sphere is easily determined) subject only to drag and gravity forces. In reality, raindrops will deform because of shear stresses as they enter the airfoil boundary layer, but, on the basis of a Weber number criterion (*33*), breakup of the drops should not occur.

Particle trajectories are determined by Newton's second law of motion. The particle equation of motion can be written in nondimensional form as

$$\frac{d\bar{\mathbf{V}}_p}{dt} = \frac{3\rho c C_D |\bar{\mathbf{V}} - \bar{\mathbf{V}}_p|}{8 r_p \rho_p} (\bar{\mathbf{V}} - \bar{\mathbf{V}}_p) + \frac{c}{\mathbf{V}_\infty^2} \bar{\mathbf{g}} \tag{2}$$

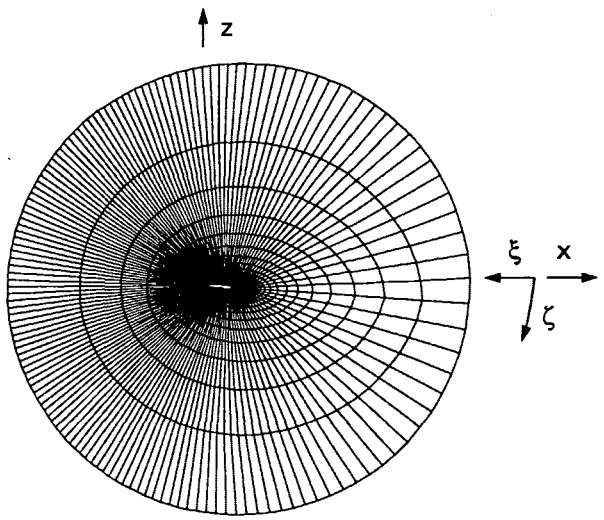

FIGURE 4 Spanwise cross section of the computational grid around a NACA 64-210 airfoil. Grid dimensions are 45 normal to the surface (ξ) by 3 spanwise (η) by 143 circumferential (ζ). *y* is spanwise.

where

$\bar{\mathbf{V}}$ and $\bar{\mathbf{V}}_p$ = air and particle velocity vectors,
ρ and ρ_p = air and particle material densities,
r_p = particle radius, and
$\bar{\mathbf{g}}$ = acceleration of gravity.

The first term on the right-hand side of Equation 2 represents the drag force acting on a particle, and the second term represents the gravitational force. For consistency with the airflow field, the variables in Equation 2 are nondimensionalized in the same manner as the Navier-Stokes equations; velocities are scaled by the free stream air velocity $\mathbf{V}_\infty$, lengths by the airfoil chord length c, and time by c/V_∞. The drag coefficient in Equation 2 can be represented over a wide range of particle Reynolds numbers by (*34*)

$$C_D = \max\{0.44, \frac{24}{Re_p}(1 + 0.15Re_p^{0.687})\} \tag{3}$$

where the particle Reynolds number is defined in terms of the nondimensional velocities $\bar{\mathbf{V}}$ and $\bar{\mathbf{V}}_p$ as

$$Re_p = \frac{\rho|\mathbf{V}_\infty(\bar{\mathbf{V}} - \bar{\mathbf{V}}_p)|2r_p}{\mu} \tag{4}$$

A second particle trajectory equation is a chain rule expression for the contravariant particle velocity

$$\frac{d\bar{\xi}_p}{dt} = \bar{\xi}_x u_p + \bar{\xi}_y v_p + \bar{\xi}_z w_p \tag{5}$$

where $\bar{\xi}_p = (\xi_p, \eta_p, \zeta_p)$ is the particle position in the curvilinear coordinate system and u_p, v_p, and w_p are the Cartesian components of the particle velocity. The metric vectors in Equation 5 are defined as

$$\bar{\xi}_x = (\xi_x, \eta_x, \zeta_x) \qquad \bar{\xi}_y = (\xi_y, \eta_y, \zeta_y) \qquad \bar{\xi}_z = (\xi_z, \eta_z, \zeta_z) \tag{6}$$

which are evaluated at the particle position through linear interpolation between the values at adjacent grid points. The subscripts x, y, and z in Equation 6 indicate partial differentiation with respect to the subscripted variable. At grid points, the metrics ξ_x, η_x, ζ_x, ξ_y, and so forth are evaluated with second-order accurate finite differences as described by Anderson et al. (*35*).

Equations 2 and 5 are two-vector, first-order ordinary differential equations that can be integrated to determine a particle trajectory. Following the example of Crowe et al. (*31*), Equation 2 is integrated analytically. Over a small time setup of particle travel, the fluid velocity and the particle Reynolds number are assumed approximately constant. Integration of Equation 2 then yields

$$\bar{\mathbf{V}}_p^{n+1} = \bar{\mathbf{V}}^n - (\bar{\mathbf{V}}^n - \bar{\mathbf{V}}_p^n)\exp(-D^n\Delta t) + \bar{\mathbf{g}}\frac{c\,[1 - \exp(-D^n\Delta t)]}{\mathbf{V}_\infty^2 D^n} \tag{7}$$

where superscripts refer to time level and

$$D^n = \frac{3\rho c C_D\,|\bar{\mathbf{V}}^n - \bar{\mathbf{V}}_p^n|}{8 r_p \rho_p} \tag{8}$$

Equation 5 is integrated numerically with a modified Euler scheme (*36*). The contravariant particle velocity, $d\bar{\xi}_p/dt$, is first calculated at the current particle position and the current time level n and then is used to predict the next particle position and contravariant velocity at time level $n + 1$. The particle position is advanced using the average of the two velocities

$$\bar{\xi}_p^{n+1} = \bar{\xi}_p^n + \left(\frac{d\bar{\xi}_p}{dt}\right)_{\text{ave}} \Delta t \tag{9}$$

with a time step based on a particle residence time of four steps in the current cell.

Modeling of Rain

The drop size distribution of natural rain can be approximated by Equation 1. For modeling purposes, this continuous spectrum of drop diameters is divided into four discrete intervals each of length $\Delta D_{p,i}$. The number density of raindrops in each interval, $N(\Delta D_{p,i})$, can be calculated by integrating Equation 1 over the interval. Then the average diameter of raindrops in the interval, $D_{p,i}$, can be determined.

Particles are entered into the computational domain from discrete locations around the boundary with an initial horizontal velocity equal to the free stream velocity $\mathbf{V}_\infty$ and an initial vertical velocity determined by equating the gravity and vertical drag forces. Each entry location j has an associated area A_j, so the raindrop number flow rate from entry location j for diameter interval $\Delta D_{p,i}$ can be expressed as

$$\dot{N}_{ij} = N(\Delta D_{p,i})\,(\bar{\mathbf{V}}_{p\infty,i} \cdot \bar{A}_j) \tag{10}$$

where $N(\Delta D_{p,i})$ is the raindrop number density for diameter interval i, and $(\bar{\mathbf{V}}_{p\infty,i} \cdot \bar{\mathbf{A}}_j)$ is the dot product of the free stream velocity of particles of average diameter $D_{p,i}$ and the normal vector to area A_j. Thus for each drop size interval $\Delta D_{p,i}$ and each entry location j, one particle of average interval diameter $D_{p,i}$ is tracked through the domain and has associated with it a raindrop number flow rate $\dot{N}_{ij}$.

Interphase Coupling

Particle drag acts as the momentum coupling between the fluid and particulate phases. It is explicitly accounted for in the particle equation of motion, but a momentum source/sink term must be added to the Navier-Stokes equations to account for the particle drag effect on fluid motion. The momentum source/sink term is determined by tabulating the particle drag throughout the flow field.

Nondimensional particle drag distributions are collected on a per volume basis for each grid cell as

$$\bar{\mathbf{F}}_{\text{drag}} = \frac{1}{V_{\text{cell}}}\sum_{i,j}\left[\frac{1}{2}\pi\frac{r_p^2}{c^2}C_D\,|\bar{\mathbf{V}} - \bar{\mathbf{V}}_p|\,(\bar{\mathbf{V}} - \bar{\mathbf{V}}_p)\right]\dot{N}_{ij}\,\Delta t_{p,ij} \tag{11}$$

where velocities are averaged over the time step, V_{cell} is the nondimensional volume of the cell (scaled by the cube of the airfoil chord length), the particle drag coefficienct C_D is determined by

Equation 3, $\dot{N}_{ij}$ is the number flow rate associated with the particle from Equation 10, and $\Delta t_{p,ij}$ is the residence time of the particle in the cell. The bracketed term in Equation 11 represents the nondimensional drag force acting on the particle, and the sum is over all particles that traverse the cell for all diameter intervals i and all particle entry locations j. The vector quantity $\overline{F}_{drag}$ determined in Equation 11 represents the coupling between the air and particle fluids and is subtracted from the right-hand side of the Navier-Stokes equations to account for the particle effect on fluid motion.

Splashback Model

Modeling of raindrop impacts on the airfoil surface presents a very complex problem, and little literature exists on the characteristics of these types of impacts. Raindrops strike the airfoil at high velocities and at angles varying from perpendicular (high-incidence impact) to nearly tangential (low-incidence impact). Some fraction of the mass of the incident drop is splashed back as droplets, and the remainder is incorporated into the liquid surface film. The fraction of mass splashed back and the diameters, initial velocities, and directions of the splashed-back droplets all affect the momentum sink experienced by the boundary layer. These characteristics of the splash are functions of the incidence angle and velocity of the incoming raindrop, and all change during the duration of splash. Obviously, it will be very difficult, if not impossible, to accurately model this phenomenon, so a relatively simple model is used. This model captures enough of the major characteristics of the splashback process that it can be used to predict, at least qualitatively, a part of the performance degradation experienced by an airfoil in rain.

Feo (*37–39*) has experimentally observed some features of the splashback process. The raindrop impact model used in particle-tracking code and shown in Figure 5 is somewhat loosely based on his observations. For a perpendicular impact (β = 90 degrees), 5 percent of the mass of the incident drop is splashed back over an angular range of θ = 120 degrees centered about the surface normal. Splashed-back droplets have a radius of 10 μm and an initial velocity equal to the velocity of the incident raindrop. For a tangential impact (β = 0 degrees), the angular range of splashback (θ), the initial velocity of the splashed-back droplets, and the fraction of the incident drop mass splashed back all go to zero, whereas the radius of a splashed-back droplet goes to 50 μm. A linear variation is assumed between these two extremes, with the splashback always centered about the surface normal.

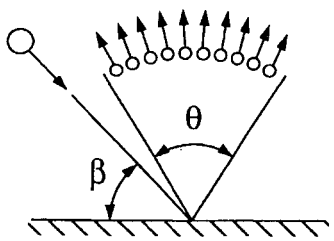

FIGURE 5 Splashback model. Droplets are splashed back over an angular range θ, which decreases linearly from 120 to 0 degrees as the incidence angle β decreases from 90 degrees for a perpendicular impact to 0 degrees for a tangential impact.

RESULTS

Numerical results are presented for a cruise-configured, 1-m chord length NACA 64-210 airfoil at a Reynolds number of Re = 2.6×10^6 (corresponding to a free stream air velocity of $V_\infty \approx$ 38 m/sec) and for rainfall rates of 0, 300, 500, and 1000 mm/hr. An eddy viscosity turbulence model (*32*) is activated near the leading edge of the airfoil to simulate a turbulent boundary layer. Turbulent particle dispersion is not considered. The airflow code does not appear to predict stall accurately for flow over the dry airfoil, so numerical results are limted to angles of attack below the stall angle of attack of 13 degrees determined experimentally (*9*).

Figure 6 shows plots of lift coefficient (c_l) versus angle of attack (α) and lift coefficient (c_l) versus drag coefficient (c_d). Wind tunnel results for the same airfoil at the same Reynolds number are also plotted. The numerical results show a decrease in lift and an increase in drag at higher angles of attack, with the penalty becoming more severe as the rainfall rate increases. Very little loss of airfoil performance is evident at low angles of attack, indicating that the loss is apparently due to premature flow separation. Although the rainfall rates used in the numerical simulations correspond to much lower LWCs than those used in the wind tunnel experiments, the performance penalty is larger, probably due to inaccuracies in the raindrop splashback model. Thus, the numerical scheme predicts a rain-induced airfoil performance penalty qualitatively similar to that measured experimentally, but the magnitude of the penalty is overpredicted.

Some features of the c_l versus c_d plot shown in Figure 6b are worth noting. First, the numerical scheme overpredicts the drag determined experimentally somewhat; lift was determined more accurately. At higher angles of attack and for a fixed value of c_l, rain causes an increase in drag. Thus the airfoil is less efficient in rain at these angles of attack. Finally, the experimental results indicate an increase in drag even at lower angles of attack that is not exhibited in the numerical results. This may be due to the effectively rougher airfoil surface, which is not modeled in the numerical scheme.

Figure 7 shows streamline patterns around the airfoil at the highest rainfall rate of 1000 mm/hr. For a rainfall rate of 1000 mm/hr, there is no separation at an angle of attack of 4 degrees, but at 8 degrees a separated region has formed near the trailing edge of the airfoil. When the angle of attack is increased to 12 degrees, massive separation has occurred on the upper surface of the airfoil and the airfoil appears to have stalled. In the absence of rain, there is no obvious separation of the flow at any angle of attack up to 12 degrees. A similar pattern could be seen for increasing rainfall rates at a constant angle of attack; as the rain increases in intensity, a separated region will grow, and the airfoil may eventually stall.

These results show a rain-induced airfoil performance penalty exhibited by a decrease in lift and an increase in drag. The performance penalty results from premature flow separation and is more severe at higher rainfall rates and higher angles of attack. Although the performance loss determined numerically shows the

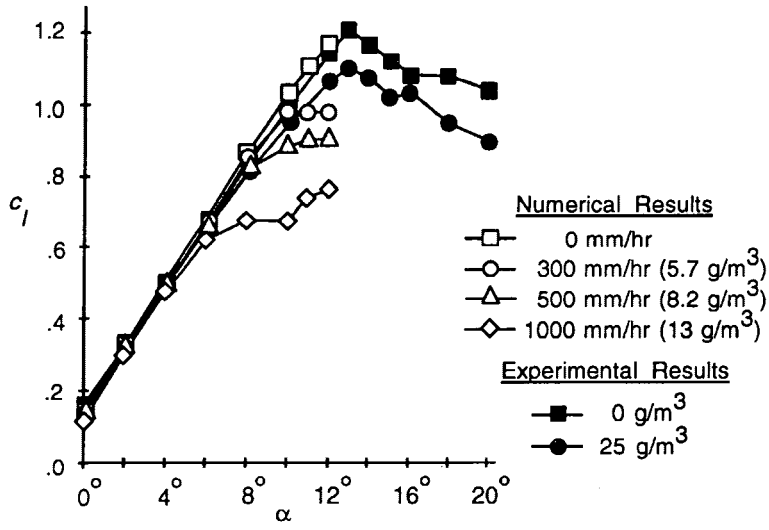

a) Lift coefficient (c_l) vs. angle of attack (α).

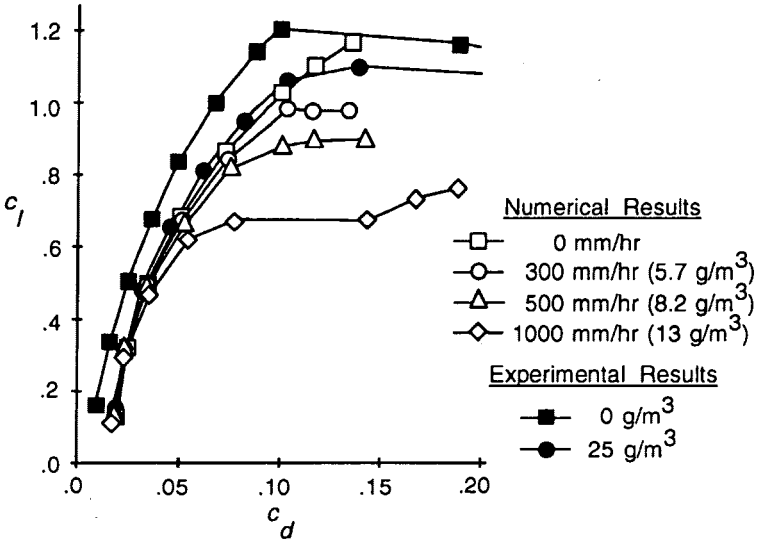

b) Lift coefficient (c_l) vs. drag coefficient (c_d).

FIGURE 6 Numerically determined plots of lift (c_l) and drag (c_d) coefficients for various rainfall rates in mm/hr with corresponding LWC shown in g/m³. Experimental results (*9*) are shown for comparison purposes.

same overall patterns that have been observed experimentally, it is greater in magnitude.

CONCLUSIONS

A particle-tracking code for an arbitrary curvilinear coordinate system has been developed and incorporated in a two-way momentum coupled scheme to numerically evaluate the performance degradation of an airfoil in heavy rain. Results show a rain-induced performance loss due to premature flow separation, although the magnitude of the loss is overestimated relative to experimental measurements. However, the method shows promise for development of a more accurate predictive tool for the evaluation of airfoil performance in rain.

Some recommendations for further research are as follows: (*a*) numerical experiments to study the effect of variations in the splashback model and possibly improve it, (*b*) revision of the airflow code or incorporation of a different code into the scheme so that stall and poststall behavior are more accurately predicted for the dry airfoil (and presumably for the airfoil in rain also), and (*c*) inclusion of the effective increase in airfoil roughness due to a water film. Variation of parameters in the model may help in the understanding of the splashback process and its role in airfoil

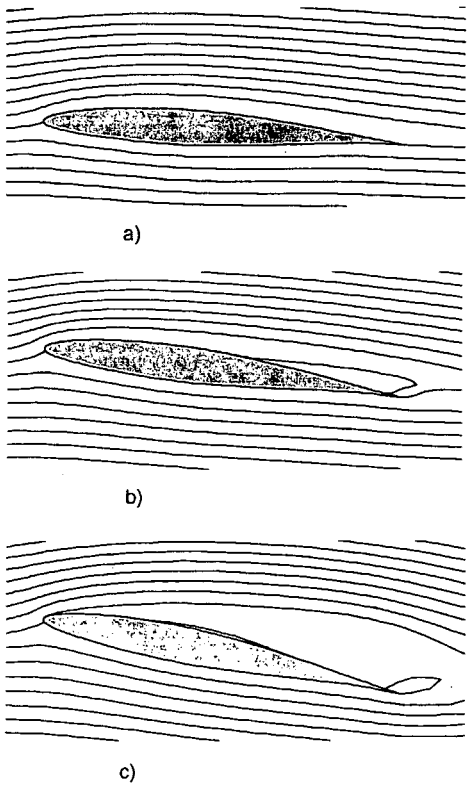

FIGURE 7 Numerically determined streamlines around an airfoil for a rainfall rate of 1000 mm/hr showing the increasing separation of the flow as the angle of attack (α) is increased: (*a*) α = 4 degrees, (*b*) α = 8 degrees, and (*c*) α = 12 degrees. Without rain, no obvious separation occurs at these angles of attack.

performance loss. To more accurately model the splashback process, experimental or analytical studies of the splashback process may be required. The apparent inability of the airflow code to accurately predict stall and poststall behavior is a problem, since premature stall is an important rain effect on airfoil performance. Finally, since the airfoil performance degradation in rain is apparently largely due to two effects, the boundary layer momentum loss to splashed-back droplets studied here and the effectively rougher airfoil surface, it may be useful to include both phenomena in the model.

It may also be advisable to educate pilots on the detrimental effect that very intense rain can have on aircraft performance. Although there seems to be an effort to train pilots in microburst avoidance and recovery techniques, the effect of the heavy rain that often accompanies a microburst appears to be largely overlooked.

ACKNOWLEDGMENTS

This paper was written for the Transportation Research Board's Graduate Research Award Program VII. The author thanks TRB for providing the opportunity to write the paper and the following people for their help and comments: Larry Jenney of TRB, Rand Decker of the University of Utah, Hubert C. Smith of Pennsylvania State University, and C. W. Kauffman of the University of Michigan. The particle-tracking code and two-phase flow model were developed under a NASA contract.

REFERENCES

1. *Aircraft Accident Report—Pan American World Airways, Inc., Clippert 759, Boeing 727-235, N43737, New Orleans International Airport, Kenner, Louisiana, July 9, 1982.* NTSB/AAR-83/02. National Transportation Safety Board, 1982.
2. *Low-Altitude Wind Shear and Its Hazard to Aviation.* National Academy Press, Washington, D.C., 1983.
3. Haines, P. A., and J. K. Luers. *Aerodynamic Penalties of Heavy Rain on a Landing Aircraft.* NASA-CR-156885. July 1982.
4. *Aircraft Accident Report—Delta Airlines, Inc., Lockheed L-1011-385-1, N726DA, Dallas/Fort Worth International Airport, Texas, August 2, 1985.* NTSB/AAR-86/05. National Transportation Safety Board, 1985.
5. Luers, J. K., and P. A. Haines. Heavy Rain Influence on Airplane Accidents. *Journal of Aircraft,* Vol. 20, No. 2, Feb. 1983, pp. 187–191.
6. Brandes, E. A., and J. W. Wilson. Measuring Storm Rainfall by Radar and Rain Gage. In *Instruments and Techniques for Thunderstorm Observation and Analysis* (E. Kesler, ed.), University of Oklahoma Press, Norman and London, 1982, pp. 171–186.
7. Horne, T. A. The Deadly Wind. *AOPA Pilot,* Aug. 1986, pp. 39–44.
8. Bilanin, A. J. Scaling Laws for Testing Airfoils Under Heavy Rainfall. *Journal of Aircraft,* Vol. 24, No. 1, Jan. 1987, pp. 31–37.
9. Bezos, G. M., R. E. Dunham, G. L. Gentry, Jr., and W. E. Melson, Jr. *Wind Tunnel Aerodynamic Characteristics of a Transport-Type Airfoil in a Simulated Heavy Rain Environment.* NASA TP-3184. Aug. 1992.
10. Hastings, E. C., Jr., and G. S. Manuel. Scale-Model Tests of Airfoils in Simulated Heavy Rain. *Journal of Aircraft,* Vol. 22, No. 6, June 1985, pp. 536–540.
11. Haines, P. A., and J. K. Luers. Aerodynamic Penalties of Heavy Rain on Landing Aircraft. *Journal of Aircraft,* Vol. 20, No. 2, Feb. 1983, pp. 111–119.
12. Riordan, P. *Weather Extremes Around the World.* Tech. Rep. 70-45-ES. U.S. Army, Jan. 1970.
13. Dunham, R. E., Jr. The Potential Influence of Rain on Airfoil Performance. *Influence of Environmental Factors on Aircraft Wing Performance.* Feb. 1987.
14. Roys, G. P., and E. Kessler. *Measurements by Aircraft of Condensed Water in Great Plains Thunderstorms.* Technical Note 49-NSSP-19. U.S. Department of Commerce, July 1966.
15. Marshall, J. S., and W. McK. Palmer. The Distribution of Raindrops with Size. *Journal of Meteorology,* Vol. 5, No. 4, Aug. 1948, pp. 165–166.
16. Joss, J., and A. Waldvogel. Raindrop Size Distribution and Sampling Size Errors. *Journal of the Atmospheric Sciences.* Vol. 26, No. 3, May 1969, pp. 566–569.
17. Rhode, R. V. *Some Effects of Rainfall on Flight of Airplanes and on Instrument Indications.* NACA TN 903. April 1941.
18. Yip, L. P. *Wind Tunnel Investigation of a Full-Scale Canard-Configured General Aviation Aircraft.* NASA TP-2382. March 1985.
19. Dwiggens, D. Dangerous When Wet? *Homebuilt Aircraft,* March 1983.
20. Hansman, R. J., Jr., and M. F. Barsotti. Surface Wetting Effects on a Laminar Flow Airfoil in Simulated Heavy Rain. *Journal of Aircraft,* Vol. 22, No. 12, Dec. 1985, pp. 1049–1053.
21. Hansman, R. J., Jr., and A. P. Craig. Low Reynolds Number Tests of NACA 64-210, NACA 0012, and Wortmann FS67-K170 Airfoils in Rain. *Journal of Aircraft,* Vol. 24, No. 8, Aug. 1987.
22. Bezos, G. M., R. E. Dunham, Jr., G. L. Gentry, Jr., and W. E. Melson. Wind Tunnel Test Results of Heavy Rain Effects on Airfoil Performance. AIAA-87-0260. Reno, Nev., Jan. 1987.
23. Campbell, B. A., and G. M. Bezos. *Steady-State and Transitional Aerodynamic Characteristics of a Wind in Simulated Heavy Rain.* NASA TP-2932. Aug. 1989.
24. Bezos, G. M., and B. A. Campbell. *Development of a Large-Scale, Outdoor, Ground-Based Test Capability for Evaluating the Effect of Rain on Airfoil Lift.* NASA TM-4420. 1993.

25. Calarese, W., and W. L. Hankey. *Numerical Analysis of Rain Effects on an Airfoil.* AIAA-84-0539. Reno, Nev., Jan. 1984.
26. Kisielewski, K. *A Numerical Investigation of Rain Effects on Lift Using a Three-Dimensional Splice Flux Vector Form of the Euler Equations.* Master's thesis. Mississippi State University, Mississippi State, 1985.
27. Donaldson, C. duP., and R. D. Sullivan. *The Effect of Heavy Rain on an Airfoil at High Lift.* NASA CR-178248. March 1987.
28. Bilanin, A. J., T. R. Quackenbush, and A. Feo. *Feasibility of Predicting Performance Degradation of Airfoils in Heavy Rain.* NASA CR-18142. June 1989.
29. Decker, R. A., and C. F. Schafer (eds.). *Mixing and Demixing Processes in Multiphase Flows with Applications to Propulsion Systems.* NASA CP-3006.
30. Durst, F., D. Milojevic, and B. Schönung. Eulerian and Lagrangian Predictions of Particulate Two-Phase Flows: A Numerical Study. *Applied Mathematical Modelling,* Vol 8, April 1984, pp. 101–115.
31. Crowe, C. T., M. D. Sharma, and D. E. Stock. The Particle-Source-in-Cell (PSI-Cell) Model for Gas-Droplet Flows. *Journal of Fluids Engineering,* Vol. 99, June 1977, pp. 325–332.
32. Hartwich, P.-M., and C.-H. Hsu. High Resolution Upwind Schemes for the Three-Dimensional Navier-Stokes Equations. *AIAA Journal,* Vol. 26, No. 11, Nov. 1988, pp. 1321–1328.
33. Wierzba, A. Deformation and Breakup of Liquid Drops in a Gas Stream at Nearly Critical Weber Numbers. *Experiments in Fluids,* Vol. 98, No. 1/2, April 1990, pp. 59–64.
34. Wallis, G. B. *One-Dimensional Two-Phase Flow.* McGraw-Hill, 1969.
35. Anderson, D. A., J. C. Tannehill, and R. H. Pletcher. *Computational Fluid Mechanics and Heat Transfer.* Hemisphere Publishing Corporation, New York, 1984, pp. 252–253.
36. Burden, R. L., and J. D. Faires. *Numerical Analysis* (3rd edition). Prindle, Weber and Schmidt, 1985.
37. Feo, A. *Rotating Arms Applied to Studies of Single Angular Drop Impacts.* AIAA-87-0257. Reno, Nev., Jan. 1987.
38. Feo, A. *Low Incidence Water Drops Splashing on Very Thin Liquid Layers Under the Influence of Thin Air Boundary Layers.* INTA Nota Tecnica N/221/510/86.013. Madrid, Spain, 1986.
39. Feo, A. *Waterdrop Splashback Characteristics of a Perpendicular Impact Near an Air Stagnation Point.* INTA Nota Tecnica N/221/501/89.025. Madrid, Spain, 1989.